# UC Davis
## UC Davis Previously Published Works

**Title**

Autophagy-linked FYVE containing protein WDFY3 interacts with TRAF6 and modulates RANKL-induced osteoclastogenesis

**Permalink**

**Authors**

Wu, Dennis J
Gu, Ran
Sarin, Ritu
et al.

**Publication Date**

**DOI**

Peer reviewed

# Autophagy-linked FYVE containing protein WDFY3 interacts with TRAF6 and modulates RANKL-induced osteoclastogenesis

**Dennis J. Wu**[a,b], **Ran Gu**[b], **Ritu Sarin**[b], **Regina Zavodovskaya**[c], **Chia-Pei Chen**[d], **Blaine A. Christiansen**[e], and **Iannis E. Adamopoulos**[a,b,f,*]

[a]Graduate Group in Immunology, University of California at Davis, United States

[b]Division of Rheumatology, Allergy and Clinical Immunology, University of California at Davis, United States

[c]Department of Anatomy, Physiology and Cell Biology, University of California at Davis, United States

[d]Department of Statistics, University of California at Davis, United States

[e]Department of Orthopedic Surgery, University of California at Davis, United States

[f]Institute for Pediatric Regenerative Medicine, Shriners Hospitals for Children, Northern California, United States

## Abstract

Recently, autophagy-related proteins were shown to regulate osteoclast mediated bone resorption, a critical process in autoimmune diseases such as rheumatoid arthritis. However, the role of autophagy-linked FYVE containing protein, WDFY3, in osteoclast biology remains elusive. WDFY3 is a master regulator in selective autophagy for clearing ubiquitinated protein aggregates and has been linked with rheumatoid arthritis. Herein, we used a series of WDFY3 transgenic mice (*Wdfy3^{lacZ}* and *Wdfy3^{loxP}*) to investigate the function of WDFY3 in osteoclast development and function. Our data demonstrate that WDFY3 is highly expressed at the growth plate of neonatal mice and is expressed in osteoclasts *in vitro* cultures. Osteoclasts derived from WDFY3 conditional knockout mice (*Wdfy3^{loxP/loxP}-LysM-Cre^+*) demonstrated increased osteoclast differentiation as evidenced by higher number and enlarged size of TRAP^+ multinucleated cells. Western blot analysis also revealed up-regulation of TRAF6 and an increase in RANKL-induced NF-κB signaling in WDFY3-deficient bone marrow-derived macrophages compared to wild type cultures. Consistent with these observations WDFY3-deficient cells also demonstrated an increase in osteoclast-related genes *Ctsk, Acp5, Mmp9* and an increase of dentine resorption in *in vitro* assays. Importantly, *in vivo* RANKL gene transfer exacerbated bone loss in WDFY3 conditional knockout mice, as evidenced by elevated serum TRAP, CTX-I and micro-CT analysis of distal femurs compared to wild type littermates. Taken together, our data highlight a novel role for

Author Manuscript Author Manuscript Author Manuscript Author Manuscript

WDFY3 in osteoclast development and function, which can be exploited for the treatment of musculoskeletal diseases.

**Keywords**

Autophagy; Autophagy-linked FYVE containing protein; WDFY3; TRAF6; Osteoclast; Musculoskeletal diseases

## 1. Introduction

Bone remodeling is a dynamic process, which maintains skeletal homeostasis and entails the removal of old bone and its replacement with new. Two types of cells with opposing functions regulate this process; the osteoclasts, that resorb bone and the osteoblasts that form new bone. Dysregulation of skeletal homeostasis leads to musculoskeletal diseases. These disorders are characterized by loss of bone and joint function that require extensive treatment and long periods of recovery. Bone destruction in musculoskeletal conditions is primarily caused by an imbalance between bone resorption and bone formation. Changes in the number and/or activity of osteoclasts/osteoblasts may be a direct reflection of musculoskeletal diseases [1] and [2].

Osteoclasts are multinucleated cells (MNCs) derived from myeloid progenitor cells. Macrophage colony-stimulating factor (M-CSF), and receptor activator of NF-κB ligand (RANKL) regulate the differentiation of osteoclasts [3]. M-CSF stimulation leads to phosphorylation of AKT and ERK, which promotes proliferation and survival in osteoclast precursor cells [4]. RANKL/RANK interaction recruits TRAF6 to activate IKKβ, which phosphorylates IκBα (inhibitor of NF-κB) and leads to its degradation. NF-κB then is released from IκBα-NF-κB complex, and translocates into the nucleus, and activates genes required for osteoclast differentiation [5]. TRAF6 has indispensable roles for osteoclastogenesis since the absence of the protein leads to osteopetrosis *in vivo* [6] and [7]. Terminally differentiated osteoclasts undergo cytoskeletal reorganization to facilitate the formation of filamentous-actin (F-actin) ring structures. The extracellular matrix, within the F-actin ring, is acidified by a vacuolar ATPase which is facilitated by carbonic anhydrase II, a crucial enzyme that acts as a proton source by catalyzing the hydration of carbon dioxide to carbonic acid [8] and [9]. Activated osteoclasts secrete bone-degrading enzymes CTSK, MMP9, TRAP into the sealing zone through the ruffled border, a specialized cellular structure that provides increased surface area to facilitate vesicles secretion [10].

WDFY proteins, WDFY1, WDFY2, WDFY3 and WDFY4, are novel proteins that contain WD40 repeats. All of WDFY family proteins contain WD40 repeats and WDFY1, 2 and 3 contain a FYVE domain, which is associated with vacuolar/lysosomal trafficking. WDFY1 and WDFY2 are medium size proteins (around 400 amino acids) and have been associated with endosomal pathway [11] and [12]. WDFY3 and WDFY4 are large proteins (>3000 amino acids) and contain PH and BEACH domains. Recently two independent genome-wide association studies revealed two SNP's rs2671692 and rs1913517 in WDFY4 associated with rheumatoid arthritis [13] and systemic lupus erythematosus [14] respectively. WDFY3 has recently been reported as a master regulator of selective autophagy [15] and [16].

Autophagy is a highly conserved cellular pathway for protein degradation. Loss of autophagy proteins has been shown to prevent joint destruction in a mouse arthritis model [17] and bone destruction in a mouse osteoporosis model [18]. Interestingly, association between WDFY3 expression and autoimmune diseases has been observed in patients with rheumatoid arthritis [19]. Moreover, WDFY3 expression has been clearly documented in human osteoclasts, the cells responsible for bone degradation [20].

WDFY3 is expressed ubiquitously and is predicted to encode for 15 isoforms. However, we found onlyWDFY3 isoform a (3508 amino acids) is expressed in bone marrow while other isoforms mainly express in other tissues such as brain and testis using NCBI database [21]. WDFY3 contains several functional domains: a Pleckstrin homology (PH) domain, a Beige and Chediak-Higashi (BEACH) domain, five WD-40 repeats, and a typical FYVE domain [22]. PH-BEACH domain containing proteins are involved in vesicle trafficking and receptor signaling. Functionally, theWDFY3 BEACH domain interacts with the adaptor protein SQSTM1 to link the cargo to the autophagic machinery and elicit directed autophagosome formation. WD-40 repeats mediate the essential interaction with ATG5 in selective autophagy and vesicle trafficking [23]. The FYVE domain functions in membrane recruitment of cytosolic proteins by binding to phosphatidylinositol 3-phosphate (PI3P). Although the role of WDFY3 in selective autophagy has been elegantly demonstrated, the role of WDFY3 in rheumatoid arthritis associated pathologies such as bone destruction remains largely unknown.

In this report, we investigate the function of WDFY3 in osteoclasts *in vitro* and *in vivo*. Our data highlight a novel role for WDFY3 in osteoclast development and function.

## 2. Methods

### 2.1. Antibodies and reagents

All cell incubations were performed in culture medium consisting of αMEM with 2 mM L-glutamine, 10% heat-inactivated FBS, 100 IU/ml Penicillin and 100 IU/ml Streptomycin (Life Technologies, 10007D). Mouse soluble RANKL (R&D Systems, 462 TR) and M-CSF ELISA (R&D Systems, DY416), RANKL ELISA (R&D Systems, DY462), and TRAF6 inhibitor (Novus, NBP2-26506) were used for *in vitro* experiments. CMG14-12 (CMG) media was generated as described before [24]. Collagenase type II (Calbiochem, 234155), dispase (Stem Cells Technologies, 07923), ascorbic acid (Sigma, A8960) and dexamethasone (Sigma, D4902) were used for osteoblast differentiation assays. AlamarBlue solution (Life Technologies, DAL1025) was used for cell viability assay. For western blot analysis and immunofluorescence staining, anti-IκBα (Cell Signaling, 4812), anti-phospho-IκBα (Cell Signaling, 2859P), anti-NF-κB p65 (Cell Signaling, 4764), and anti-phospho-NF-κB p65 (Cell Signaling, 3033P), anti-Src (Millipore, 05–184), and phospho-Src (Millipore, 07–909), anti-WDFY3 (Novus, NBP1-03332), anti-TRAF6 (Santa Cruz Biotechnology, clone D-10), anti-β-actin antibody (Cell Signaling, 4970), 800 or 680 secondary antibodies (Li-Cor). For flow cytometry, APC anti-mouse c-Fms and PE anti-RANK antibodies (Biolegend) were used for cell staining.

## 2.2. Mice and bone cell culture

Animal experiments were conducted in accordance with the protocol approved by the Institutional Animal Care and Use Committee of the University of California, Davis. Eight to twelve weeks old C57BL/6 (The Jackson Laboratory), $Wdfy3^{lacZ/+}$, $Wdfy3^{loxP/loxP}$-$LysM$-$Cre$+, $Wdfy3^{loxP/loxP}$ animals were sacrificed to extract bone marrow from both rear femurs and tibias bones. Generation of $Wdfy3^{lacZ}$, $Wdfy3^{loxP}$ animals is described in previous study [25]. Bone marrow cells were cultured with 1:20 (v/v) CMG media in absence or presence of 30 ng/mL RANKL. Media and cytokines were exchanged every other day. For X-gal staining, neonate C57BL/6 or $Wdfy3^{lacZ/+}$ were sacrificed and sectioned for histology.

For osteoblast culture, cells were isolated from $Wdfy3$-$cKO$ or wild type newborn mice calvaria by three sequential collagenase/dispase digestions. Primary osteoblasts were expended in αMEM with 2 mM L-glutamine, 10% heat-inactivated FBS, 100 IU/ml penicillin, and 100 IU/ml streptomycin until they were confluent before any use. Upon confluence, cells were seeded at $1 \times 10^5$ cells/well in 6-well plate, and stimulated with 50 μg/ml ascorbic acid, and 10 nM dexamethasone. For alkaline phosphatase (ALP) activity assay, cells were lysed in 100 μl of 10 mM Tris-HCl. Total cell lysates were incubated with 15 mM $p$-Nitrophenylphosphate (pNPP) (Sigma, P4744) at 37 °C for 30 min, and ALP activity was measured by spectrophotometer. Protein concentrations were analyzed by BCA assay (Thermo Scientific, 23227).

## 2.3. X-gal staining for β-galactosidase

Staining for β-galactosidase activity indicating $Wdfy3^{lacZ}$ expression on embryos sections as well as cells cultured on coverslips. Detergent rinse buffer (100 mM Sodium phosphate, 2 mM Magnesium chloride, 0.01% Sodium deoxycholate, 0.02% nonidet-P-40) was used to remove excess Tissue-Tek® OCT compound on slides. Slides were incubated in X-gal staining solution (1 mg/ml X-gal, 5 mM potassium ferricyanide, 5 mM potassium ferryocyanide) overnight at room temperature. Fast red nuclear stain (Vector Labs) was used to counter stain nuclei in cell bone marrow cell culture. Fluoromount-G (Southern Biotech, 0100-01) was used to mount sample with cover glasses.

## 2.4. RNA extraction and real-time quantitative PCR

Total RNA was purified from different stages of osteoclast cultures using the RNAeasy Mini Kit (Qiagen). Gene expression was calculated using the $2^{-\Delta Ct}$ method. qPCR primers used in the study: $Ctsk$ forward 5′- AAGTGGTTCAGAAGATGACGGGAC-3′, reverse 5′-TCTTCA-GAGTCAATGCCTCCGTTC, $Mmp9$ forward 5′-AATCTCTTCTA.

GAGACTGGG-AAGGAG-3′, reverse 5′-AGCTGATTGACTAAAG-TAGCTGGA-3′, $Acp5$ forward, 5′-AGCAGCCAAGGAGGACTACGTT-3′, reverse 5′-TCGTTGATGT CGCACAGAGG-3′, $Wdfy3$ forward 5′-TCATCAGAGTCCACCGTGAG-3′, reverse 5′-CCACT-TGCCCCTCA-TAAAAA-3′, β$2M$, forward 5′- CTGCTACGTAACACAGTT CCACCC-3′, reverse 5′- CATGATGCTTGATCACATGTCTCG-3′.

### 2.5. Assessment of osteoclast formation

TRAP staining was performed according to manufacture's instruction with Acid phosphatase, Leukocyte (TRAP) Kit (Sigma, 387A). Briefly, macrophages or mature osteoclasts were first fixed in the acetone with citrate. Naphthol AS-BI phosphate was added as substrate for TRAP and produce insoluble pink dye. Cells grew on glass coverslips were fixed with 4% formaldehyde for 5 min and then permeabilized for 6 min in 0.5% Triton X-100 (in PBS) and rinsed with PBS to detect F-actin ring structure. The cells on coverslips were then incubated with phalloidin for 30 min, washed and rinsed with PBS before mounted with DAPI (Vector Laboratories, H1200), and observed using a fluorescence microscope (Nikon). Functional evidence of osteoclast formation was determined by a lacunar resorption assay system using cell cultures on dentine slices as previously described [26]. Cells were removed from the dentine slices by treatment with 10% Triton-X with sonication. The dentine slices were washed in distilled water and ultrasonicated to remove adherent cells, then stained with 1% (v/v) toluidine blue to reveal areas of lacunar resorption and examined by light microscopy. The pit area was quantified using NIH image analysis program ImageJ.

### 2.6. Scanning electron microscopy (SEM)

Functional evidence of osteoclast differentiation was obtained by a lacunar resorption assay system in which cells are cultured on dentine slices as previously described [27]. Dentine provides a smooth-surface mineralized substrate for the identification of lacunar resorption pits, which are only formed by osteoclasts. After BMMs were cultured on dentine slices for 7–10 days, the slices were removed from the wells and fixed in 4% glutaraldehyde or cells were removed from the dentine slices by treatment with 10% Triton-X with sonication. The dentine slices were dehydrated by passing through graded alcohols and then through graded hexamethyldisilazane solution (Electron Microscopy Sciences, 16700) before being air-dried. Dentine slices were then mounted onto aluminum stubs using double-sided carbon adhesive tabs, sputter-coated with gold and examined using a Philips XL30 TMP scanning electron microscope.

### 2.7. Immunofluorescence staining

Osteoclasts grown on coverslip were imaged by Nikon C1 confocal microscopy after fixation in 4% paraformaldehyde for 10 min. Cells were permeabilized in 0.2% Triton X-100 and blocked with 10% normal donkey serum buffer in PBS for 2 h at room temperature. All antibodies were diluted in 5% normal donkey serum buffer in PBS. Primary antibodies were applied on samples overnight at 4 °C. Secondary antibody AF-488 donkey and anti-mouse Ig or AF-594 donkey anti-rabbit Ig antibodies were added to samples for 1 h incubation at room temperature. TRITC conjugated phalloidin was used for F-actin staining for 30 min incubation at room temperature. Coverslips were then mounted in mounting media with DAPI (Vector Laboratories, H1200) to stain nuclei. The size of multinucleated cell was quantified using NIH image analysis program ImageJ.

### 2.8. Co-immunoprecipitation

Osteoclast-like cells cultured from 8 to 12 weeks old wild type mice were lysed in lysis buffer consisting of 50 mM Tris-HCl pH 7.4, 150 mM NaCl, 1 mM EDTA, 1% v/v Triton X-100 containing protease inhibitor cocktail tablet (Roche, 4693124001). The clear lysate was incubated with anti-Wdfy3 antibody overnight and was then Co-immunoprecipitated by dynabeads protein A immunoprecipitation kit (Life technologies, 10006D).

### 2.9. Western analysis

Bone marrow-derived macrophages and osteoclast-like cells starved in serum-free medium were stimulated with RANKL (100 ng/ml) or M-CSF (100 ng/ml) and lysed at indicated time points. Protein lysates obtained from cell cultures were run on a Nu-Page 3–8% Tris-Acetate gel, 4–12% Bis-Tris gel or 12% Bis-Tris gels (Invitrogen). Proteins were transferred to PVDF membranes and blocked in Odyssey blocking buffer. Membranes were incubated with anti-Wdfy3 primary antibody diluted in Odyssey blocking buffer containing 0.1% Tween-20, overnight at 4 °C. After washing, we incubated with secondary antibody (Li-Cor) in blocking buffer containing 0.1% Tween-20 and 0.02% SDS, washed, and imaged on the Li-Cor Odyssey scanner. The process was repeated with β-actin as loading control. Signal intensity relative to background was determined using Li-Cor Image Studio software.

### 2.10. Microarray analysis

Total RNA was amplified and purified using an Ambion Illumina RNA amplification kit (Ambion) to yield biotinylated cRNA and 1.5 μg of cRNA samples were hybridized to Illumina WG-6 v2.0 chips according to manufacturer's instructions. Arrays were scanned by Illumina iScan. Raw data were extracted using the software provided by the manufacturer (Illumina GenomeStudio). Probe signal value was transformed by mean normalization and logarithm, and then illustrated by heat map. Go-ontology analysis for the list of significant probes was performed using PANTHER (http://www.pantherdb.org/panther/ontologies.jsp), using text files containing gene.

### 2.11. Flow cytometry of bone marrow derived macrophages

Bone marrow cells were isolated from *Wdfy3-cKO* or wild type mice and were cultured with 1:20 (v/v) CMG media for 4 days. Non-specific binding was blocked by pretreating cells with rat anti-mouse CD16/32 mAb (Biolegend, clone 93) for 10 min on ice. Cells were stained using predetermined optimized mAb concentration, and events were collected on a FACSAriaII flow cytometer (BD Biosciences) and were analyzed using FlowJo software (Tree Star).

### 2.12. RANKL gene transfer model

RANKL gene transfer was performed as described previously [28]. Briefly, 5 μg of RANKL or GFP minicircles were delivered to experimental mice in ~10% of mice body weight of warm Ringer's solution via tail veins in 5–7 s. The soluble RANKL level in serum was monitored using mouse RANKL ELISA. Serum TRACP 5b was monitored by MouseTRAP EIA assay (Immunodiagnostic System, SB-TR103) and serum CTX-I was measured by RatLaps (CTX-I) EIA assay (Immunodiagnostic System, AC-06F1).

### 2.13. Trabecular bone analysis by micro-computed tomography imaging

Fixed mouse skeletons were imaged at the Center for Molecular and Genomic Imaging (UC Davis) in order to visualize full-body skeletal structure. Mouse skeletons were imaged in ethanol in 50 mL conical vials. The vials were secured in place using a custom plastic holder to prevent any movement during the scan. X-ray tomographic images were obtained on the MicroXCT-200 specimen CT scanner (Carl Zeiss X-ray Microscopy) using the Xradia LE3 filter, 40 kV voltage, 200 μA current, with 800 projections over 360°, 3 s per projection. The camera pixels were binned by 2 providing a $1024 \times 1024$ pixel arrayed projection. The source-detector configuration resulted in an isotropic voxel size of 30.2354 μm. The tomographic image was reconstructed with a center shift (−0.41 pixels) and beam hardening parameter value of 0.1 to obtain optimally reconstructed images. A smoothing filter of kernel size 0.8 was applied during reconstruction. Images were reconstructed into 16-bit values.

Distal femurs were imaged with micro-computed tomography (SCANCO μCT 35) to quantify trabecular bone structure in the distal femoral metaphysis. Dissected limbs were fixed in 4% paraformaldehyde for 24–48 h, and then transferred to 70% ethanol. Knees were scanned according to the guidelines for micro-computed tomography (μCT) analysis of rodent bone structure [29] (X-ray tube potential = 55 kVp, intensity = 114 μA, 6 μm isotropic nominal voxel size, integration time = 900 ms, number of projections = 1000/180°). Trabecular bone of the distal femoral metaphysis was analyzed by manually drawing contours on 2D transverse slices. The volume of interest was 0.9 mm (150 slices) immediately adjacent to the distal epiphyseal growth plate. Trabecular bone was segmented from non-bone using a global threshold of 543.9 mg HA/cm$^3$; this threshold was determined based on histograms of pixel brightness for the volumes of interest and visual comparison with unsegmented images. We quantified trabecular bone volume fraction (BV/TV), trabecular thickness (Tb.Th), trabecular number (Tb.N), apparent bone mineral density (Apparent vBMD; mg HA/cm$^3$ TV) and other parameters using the manufacturer's analysis tools.

### 2.14. Statistical analyses

Statistical significance was determined using Student's *t*-test and *p*-values lower than 0.05 were considered significant.

## 3. Results

### 3.1. WDFY3 is expressed in bone tissue and osteoclasts

To analyze the expression of WDFY3 in bone tissue, we employed a *Wdfy3$^{lacZ}$* line previously generated by gene targeting [25] to help us identify β-gal$^+$/Wdfy3$^+$ cells. X-gal staining of the proximal aspect of the humerus bone sections obtained from newborn (P3) heterozygote pups revealed the presence of β-gal, which indicated Wdfy3 expression, in the periosteum, cartilage, growth plate, trabeculae of the primary spongiosa, and scattered hematopoietic cells within the medullary cavity (Fig. 1A, middle panel). Interestingly, β-gal$^+$/Wdfy3$^+$ cells concentrate at the trabeculae (Tr) but are less prominent in the hypertrophic zone (HZ) (Fig. 1A, right panel). No β-gal staining was detected as expected in

the control wild type tissue sections (Fig. 1A, left panel). Furthermore, we performed *in vitro* macrophage and osteoclast cultures where again X-gal staining also revealed the expression of β-gal⁺/WDFY3⁺ on bone marrow-derived macrophages (BMMs) and multinucleated giant cells cultured from $Wdfy3^{+/lacZ}$ heterozygote animals' bone marrow (Fig. 1B, right panel) but not in the wild type cells (Fig. 1B, left panel). We also observed β-gal⁺/WDFY3⁺ expression in osteoblasts and their precursor cells cultured from P3 $Wdfy3^{+/lacZ}$ heterozygote animals' calvarias (Supplementary Fig. 1A, right panel) but not in the wild type cells (Supplementary Fig. 1A, left panel).

In order to conditionally delete WDFY3 in osteoclasts and their precursor cells, $Wdfy3^{loxP}$ transgenic mice were crossed to homozygosity and bred to mice that express Cre recombinase under the control of the ubiquitously myeloid lineage expressed *Lysozyme 2* gene (*LysM-Cre*) and the $Wdfy3^{loxP/loxP}$-*LysM-Cre* mice (referred as *Wdfy3-cKO* mice in this manuscript). The loss of WDFY3 in our *Wdfy3-cKO* was verified by western blotting on isolated myeloid cells where ~85% of WDFY3 is knocked out in mutant animals compared to wild type animals (Fig. 1C). Immunofluorescence staining demonstrated a ubiquitous expression of WDFY3 (green) in wild type BMMs and multinucleated giant cells (Fig. 1E, H). We observed WDFY3 expression in the cytosol, which also localized at the edge of filamentous actin ring (red) structures in the wild type multinucleated giant cells (Fig. 1H). We observed minimal WDFY3 (green) signal in *Wdfy3-cKO* cells, which may be due to non-specific binding of the antibody (Fig. 1F, I) and did not observe WDFY3 signal in the wild type cells stained with isotype control (Fig. 1D, G).

## 3.2. Loss of WDFY3 does not alter cell viability in bone marrow-derived macrophages

Next, we investigated whether WDFY3 deficiency influences osteoclast precursor cells. Interestingly, we did not observe any differences between *Wdfy3-cKO* and wild type BMMs in the survival of osteoclast precursor populations, or expression of protein in c-Fms and RANK receptors as evidenced by alamar blue assay (Fig. 2A) and flow cytometric analysis (Fig. 2B). Phosphorylation of AKT and ERK, associated with cell survival pathways, was also similar between WDFY3-deficient and wild type BMMs in time-course stimulation with 100 ng/ml M-CSF (Fig. 2C). To identify potential differences in macrophages and osteoclasts derived from *Wdfy3-cKO* and wild type cultures, we performed microarray analysis on *Wdfy3-cKO* and wild type cultures treated with or without RANKL.

In agreement with our data generated by flow cytometry, western blotting and survival assays we did not observe significant differences in macrophage cultures using the Illumina WG-6 v2.0 chip (data not shown). However, WDFY3-deficient BMMs *ActB, Cx3cr1, Lcn2, Lyz* and *Pglyrp1* gene expression were different from wild type BMMs. Interestingly, we observed down-regulation of genes associated with cytoskeleton, extracellular matrix, and metabolic pathways in *Wdfy3-cKO* BMM culture treated with RANKL compared to wild type culture (Fig. 2D). As these genes are critical for osteoclast function we next performed osteoclast functional assays.

### 3.3. Loss of WDFY3 in myeloid cells leads to enhanced osteoclastogenesis in vitro

In osteoclast assays, bone marrow-derived macrophages were treated for 5 days with 30 ng/ml of RANKL. WDFY3 deficiency resulted in earlier formation of TRAP$^+$ cells compared to wild type cultures (Fig. 3A, B, K). Furthermore, consistent with this enhanced osteoclastogenesis we observed that WDFY3-deficient cells also formed larger multi-nucleated TRAP$^+$ cells in 7-day cultures compared to wild type cells (Fig. 3C, D, L). In addition to the increased size of TRAP$^+$ multinucleated cells (MNCs), *Wdfy3-cKO* also were capable of F-actin ring formation and had larger cell perimeters (Fig. 3E, F, M).

To access osteoclast function, and observe detailed morphological differences, we further cultured BMMs on dentin slices and visualized with scanning electron microscopy (SEM). Osteoclasts cultured from wild type or *Wdfy3-cKO* mice were large (~200 μm), flattened, and spread over the dentine surface to which they were attached by fine microvilli (Fig. 3G and H). Lacunar resorption was noted after 10 days of treatment with RANKL; in the absence of RANKL, no lacunar resorption was detected. Interestingly, *Wdfy3-cKO* osteoclasts demonstrated increased activity in dentine resorption assays compared to wild type osteoclasts (Fig. 3I, J, N). In agreement with these observations, gene expression data also demonstrated an increase in osteoclast specific genes including *Ctsk, Mmp9, Acp5, Nfatc1*, and *Itgb3* (Fig. 3O). No significant changes were observed in *p62*, autophagy-related genes *Atg5* and *Atg7*, and deubiquitinase gene *Cyld* in WDFY3-deficient cells compared to wild type cells (Supplementary Fig. 2).

### 3.4. WDFY3 modulates NF-κB activity via up-regulation of TRAF6

Since we observed enhanced osteoclastogenesis in our *in vitro* assays, we hypothesized that loss of WDFY3 might affect the RANKL signaling pathway which is the major pathway for osteoclast differentiation and function. We first cultured bone marrow cells from *Wdfy3-cKO* or wild type mice in the presence of M-CSF and performed a dose response 0, 7.5, 15 and 30 ng/ml of mouse sRANKL (Fig. 4A). We observed increased osteoclast differentiation in the presence of low dose RANKL in WDFY3-deficient BMMs compared to wild type cells. In keeping with these data, total cell lysates from WDFY3-deficient multinucleated giant cells stimulated with RANKL (100 ng/ml) also demonstrated enhanced phosphorylated IκBα degradation and increased phosphorylated NF-κB p65 after 5 min of RANKL stimulation (Fig. 4B). Src phosphorylation patterns demonstrated no significant differences between *Wdfy3-cKO* and wild type mice (Fig. 4B). Consistent with RANKL-hyperactivation in WDFY3-deficient BMMs we also observed a discrepancy in the expression of TRAF6 at both message and protein level between WDFY3-deficient cells compared to wild type cells cultured in the presence of RANKL (Fig. 4C, D).

### 3.5. WDFY3 interacts with TRAF6 in TRAP$^+$ MNCs

To investigate the interaction of WDFY3 and TRAF6 in osteoclasts, we performed WDFY3 co-immunoprecipitation (co-IP) of total cell lysates derived from RANKL-treated cultures and immunoblotted with anti-WDFY3 and anti-TRAF6 specific antibodies. Our results indicated an interaction of WDFY3 and TRAF6 in MNCs (Fig. 5A). To further examine these interactions, we labeled BMMs and multinucleated giant cells with immunofluorescence antibodies, anti-WDFY3 (red), anti-TRAF6 (green), and DAPI (blue),

and examined the cells under confocal microscopes. In agreement with the co-IP data, we observed that WDFY3 and TRAF6 co-localize in both cell types (Fig. 5B and C). Collectively, these findings confirm WDFY3 and TRAF6 interaction in the bone marrow-derived macrophages and multinucleated giant cells. To examine whether the increased osteoclast differentiation in WDFY3-deficient cells is TRAF6 dependent, we treated wild-type or WDFY3-deficient osteoclast culture with TRAF6 inhibitor at 25, 50, 100 μM (Fig. 5D). We observed a dose dependent reduction of TRAP$^+$ MNCs (Fig. 5E) that suggested the enhanced osteoclast differentiation in WDFY3-deficient cells is TRAF6 dependent.

### 3.6. Loss of WDFY3 exacerbates bone loss in the RANKL gene transfer model

To address the role of WDFY3 in osteoclast differentiation and function *in vivo*, we used RANKL gene transfer to overexpress RANKL *in vivo* as previously described [28]. RANKL-gene transfer induced similar systemic levels of serum RANKL in both *Wdfy3-cKO* and wild type littermates at day 7-post gene transfer (Fig. 6A). However, despite the equal serum levels of RANKL we detected a marked increase in serum TRACP 5b, which correlated with higher numbers of osteoclasts, and CTX-I, a bone resorption marker, in comparison to GFP gene transfer animals at day 7-post gene transfer (Fig. 6B, C). To identify a functional significance of these changes we performed whole body MicroCT scans, where we observed reduced bone density (Fig. 6D). To evaluate these findings, we performed quantitative high resolution MicroCT analysis at distal femurs of *Wdfy3-cKO* mice and compared to wild type littermates at day 30-post gene transfer. We found that trabecular bone volume fraction (BV/TV) was decreased and trabecular separation (Tb. Sp) was increased significantly in RANKL gene transfer *Wdfy3-cKO* compared to wild type littermates 30 days post gene transfer. We also observed a trend towards decreased trabecular thickness (Tb. Th) ($p = 0.2112$), and trabecular number (Tb. N) ($p = 0.2038$) in RANKL gene transfer *Wdfy3-cKO* compared to wild type (Fig. 6E–I). Moreover, we found no difference between WDFY3-deficient osteoblast cultures compare to wild type osteoblast cultures by ALP staining (Supplementary Fig. 1B) and ALP activity assay (Supplementary Fig. 1C). Collectively, these findings confirmed loss of WDFY3 leads to exacerbated bone resorption compared to wild type mice *in vivo*.

## 4. Discussion

The ubiquitin-proteasome system (UPS) and autophagy are the two main protein degradation pathways in mammalian cells. In the UPS system, damaged or unwanted proteins are labeled with ubiquitin and later degraded by the proteasome [30]. During autophagy, damaged or unwanted proteins are recruited into an autophagosome, which subsequently fuses with lysosomes to form an autolysosome, where protein degradation takes in place [31]. Although autophagy has been considered to be non-selective process, accumulating recent evidence demonstrate that autophagy also encompasses highly selective degradation processes with high specificity such as clearing damaged mitochondria (mitophagy) and clearing ubiquitinated protein aggregates (aggrephagy) [32]. WDFY3, also known as autophagy-linked FYVE containing protein (ALFY), is a highly conserved and ubiquitously expressed protein across species that plays an essential role in selective autophagy [22]. In selective autophagy, WDFY3 forms a complex with Sequestosome1

(SQSTM1) to recruit ubiquitinated protein aggregates. The WDFY3/SQSTM1 complex also recruits the autophagy related protein 7 (ATG7) activated ATG5-ATG12 complex, and ATG7 lapidated LC3II to form an autophagosome which subsequently fuses with the lysosome (autolysosome) for protein degradation [15] [16], and [23]. Interestingly, deficiency in ATG5 or ATG7 in mice leads to impaired ruffled border formation in osteoclasts, leading to defective secretory function and reduced bone resorption independently from their known function in autophagy [18]. Similarly, a mutation in WDFY3 in mice had no detectable difference in autophagosome formation and ubiquitinated protein expression in developmental brain compared to wild type mice [25]. In keeping with these observations we did not observe difference in autophagy-related gene expression nor starvation-induced autophagy (data not shown) between WDFY3-deficient and wild type pre-osteoclasts. These data suggest that WDFY3 may also have autophagy independent roles in osteoclast biology similar to the aforementioned ATG5/7 proteins, which merits further investigation.

Deficiency in WDFY3 orthologues in mice and *Drosophila* has been associated with neurodegenerative and developmental disorders [25] and [33]. While multiple WDFY3 isoforms are predicted, their function is yet to be elucidated and it is not clear whether WDFY3 has other roles beyond selective autophagy and may contribute to diseases of the musculoskeletal system. This is particularly important as recent clinical studies suggested that WDFY3 also regulates the survival of rheumatoid arthritis synovial fibroblasts, which is paramount in pannus formation and synovial inflammation in rheumatic diseases [19]. Other groups have shown WDFY3 co-localized with SQSTM1, a protein implicated in Paget's disease of bone, in human osteoclasts [20]. Due to these observations we investigated the expression of WDFY3 using *Wdfy3^lacZ^* mice, and found that indeed WDFY3 is expressed in both osteoclasts and osteoblasts and its prominently expressed within the growth plate which is the most active bone remodeling site.

WDFY3 deficiency resulted in an increased osteoclast differentiation and activation compared to wild type cells using functional osteoclast assays. In agreement with these functional assays, we also observed up-regulation of osteoclast specific genes *Ctsk, Mmp9*, and *Acp5* in WDFY3-deficient cells compared to wild type cells. The increased osteoclast differentiation was not due to variations of c-Fms, RANK expression that might sensitize a specific population to proliferation or differentiation signals. This was further confirmed in our survival and viability assays in WDFY3-deficient osteoclast precursor cells. Instead, the increased osteoclast differentiation could be due to an up-regulation of TRAF6 accompanied by enhanced NF-κB signaling in WDFY3-deficient osteoclasts. We then further confirmed Wdfy3 and TRAF6 interaction in the osteoclasts which is in agreement with another group's findings in HeLa cells where WDFY3 forms complex with TRAF6 for midbody ring degradation by selective autophagy [34]. Our observation of WDFY3 role in TRAF6-dependent osteoclast differentiation is interesting as TRAF6 also regulates IL-1 and TLR signaling pathways where TRAF6 binds to IRAK family members such as IRAK 1, 2, 4 and leads to NF-κB activation [7] and [35]. Although we did not observe difference in IRAK family members expression between *Wdfy3-cKO* and wild type mice in our microarray analysis, it remains a possibility that higher level of TRAF6 in *Wdfy3-cKO* mice may also contribute to activation of innate immunity that required further studies.

Using a newly developed *in vivo* RANKL gene transfer model [28], we further identified increased bone loss in *Wdfy3-cKO* mice post RANKL gene transfer by high resolution MicroCT analysis accompanied with up-regulation of serum TRACP 5b (which correlated to a higher number of osteoclasts), and CTX-I (a bone resorption marker) compared to wild type littermates. These observations were most likely not caused by reduced bone formation since we did not observe any difference between WDFY3-deficient osteoblasts and the wild type cells in our osteoblast functional assays as shown in our Supplementary data. The increased osteoclast activation in *Wdfy3-cKO* mice demonstrated close resemblance with CYLD$^{-/-}$ mice, where loss of deubiquitinase CYLD led to osteopenia due to constant activation of TRAF6 [36]. We did not observe WDFY3-deficient cells altered *Cyld* expression at the mRNA level, which suggests Wdfy3 may be a novel negative regulator in RANKL signaling pathway.

Apart from the regulation of TRAF6 in osteoclasts, WDFY3-deficient osteoclasts demonstrated a down-regulation of cytoskeleton genes *Acta1, Actn2, Tnni2* and *Tcap* in our microarray analysis. This is interestingly similar to a recent human synovium microarray analysis that demonstrated down-regulation of *Acta1, Actn2 Tnni2*, and *Tcap* in rheumatoid arthritis (RA) patients compared to spondylarthritis (SpA) patients [37]. WDFY3-deficient osteoclasts also exhibited a down-regulation of several extracellular matrix protein genes including *Mmp2*. This is also intriguing as mutation or loss of *Mmp2* have been implicated in inflammatory arthritis and bone destruction [38] and [39]. Furthermore, we also observed a downregulation of metabolic pathway genes and extracellular matrix genes such as *Car3* (carbonic anhydrase 3) and *Sparc* (Osteonectin) with possible roles in musculoskeletal diseases [40] and [41]. However these gene expression profiles and their functional roles merit further investigation.

Collectively, our data provide a novel association between WDFY3 and the RANKL-induced osteoclastogenesis pathway via the modulation of TRAF6. Such regulation of osteoclast formation via WDFY3 can be critical for understanding and designing the therapeutic interventions for the treatments of rheumatoid arthritis and other musculoskeletal disorders.

## Supplementary Material

Refer to Web version on PubMed Central for supplementary material.

## Acknowledgments

## Abbreviations

| | |
|---|---|
| **ALP** | alkaline phosphatase |

| **Atg5 and Atg7** | Autophagy-related proteins 5 and 7 |
| **BEACH** | Beige and Chediak-Higashi |
| **co-IP** | co-immunoprecipitation |
| **F-actin** | filamentous-actin |
| **Flp** | flippase |
| **M-CSF** | Macrophage colony-stimulating factor |
| **MNCs** | multinucleated cells |
| **PI3P** | phosphatidylinositol 3-phosphate |
| **PH** | Pleckstrin homology |
| **RANKL** | receptor activator of NF-$\kappa$B ligand |
| **BV/TV** | trabecular bone volume fraction |
| **Tb. N** | trabecular number |
| **Tb. Th** | trabecular thickness |
| **Tb. Sp** | trabecular separation |

# References

1. Schett G, Gravallese E. Bone erosion in rheumatoid arthritis: mechanisms, diagnosis and treatment. Nat. Rev. Rheumatol. 2012; 8:656–664. [PubMed: 23007741]

2. Edwards JR, Mundy GR. Advances in osteoclast biology: old findings and new insights from mouse models. Nat. Rev. Rheumatol. 2011; 7:235–243. [PubMed: 21386794]

3. Lacey DL, Timms E, Tan HL, Kelley MJ, Dunstan CR, Burgess T, et al. Osteoprotegerin ligand is a cytokine that regulates osteoclast differentiation and activation. Cell. 1998; 93:165–176. [PubMed: 9568710]

4. Ross FP. M-CSF, c-Fms, and signaling in osteoclasts and their precursors. Ann. N. Y. Acad. Sci. 2006; 1068:110–116. [PubMed: 16831911]

5. Henkel T, Machleidt T, Alkalay I, Kronke M, Ben-Neriah Y, Baeuerle PA. Rapid proteolysis of I kappa B-alpha is necessary for activation of transcription factor NF-kappa B. Nature. 1993; 365:182–185. [PubMed: 8371761]

6. Naito A, Azuma S, Tanaka S, Miyazaki T, Takaki S, Takatsu K, et al. Severe osteopetrosis, defective interleukin-1 signalling and lymph node organogenesis in TRAF6-deficient mice. Genes Cells: Devoted Mol. Cell. Mech. 1999; 4:353–362.

7. Lomaga MA, Yeh WC, Sarosi I, Duncan GS, Furlonger C, Ho A, et al. TRAF6 deficiency results in osteopetrosis and defective interleukin-1, CD40, and LPS signaling. Genes Dev. 1999; 13:1015–1024. [PubMed: 10215628]

8. Vaananen HK, Karhukorpi EK, Sundquist K, Wallmark B, Roininen I, Hentunen T, et al. Evidence for the presence of a proton pump of the vacuolar H(+)-ATPase type in the ruffled borders of osteoclasts. J. Cell Biol. 1990; 111:1305–1311. [PubMed: 2144003]

9. Lehenkari P, Hentunen TA, Laitala-Leinonen T, Tuukkanen J, Vaananen HK. Carbonic anhydrase II plays a major role in osteoclast differentiation and bone resorption by effecting the steady state intracellular pH and Ca2+ Exp. Cell Res. 1998; 242:128–137. [PubMed: 9665810]

10. Teitelbaum SL. The osteoclast and its unique cytoskeleton. Ann. N. Y. Acad. Sci. 2011; 1240:14–17. [PubMed: 22172034]

11. Hu YH, Zhang Y, Jiang LQ, Wang S, Lei CQ, Sun MS, et al. WDFY1 mediates TLR3/4 signaling by recruiting TRIF. EMBO Rep. 2015; 16:447–455. [PubMed: 25736436]

12. Hayakawa A, Leonard D, Murphy S, Hayes S, Soto M, Fogarty K, et al. The WD40 and FYVE domain containing protein 2 defines a class of early endosomes necessary for endocytosis. Proc. Natl. Acad. Sci. U. S. A. 2006; 103:11928–11933. [PubMed: 16873553]

13. Okada Y, Wu D, Trynka G, Raj T, Terao C, Ikari K, et al. Genetics of rheumatoid arthritis contributes to biology and drug discovery. Nature. 2014; 506:376–381. [PubMed: 24390342]

14. Han JW, Zheng HF, Cui Y, Sun LD, Ye DQ, Hu Z, et al. Genome-wide association study in a Chinese Han population identifies nine new susceptibility loci for systemic lupus erythematosus. Nat. Genet. 2009; 41:1234–1237. [PubMed: 19838193]

15. Simonsen A, Birkeland HC, Gillooly DJ, Mizushima N, Kuma A, Yoshimori T, et al. Alfy, a novel FYVE-domain-containing protein associated with protein granules and autophagic membranes. J. Cell Sci. 2004; 117:4239–4251. [PubMed: 15292400]

16. Filimonenko M, Isakson P, Finley KD, Anderson M, Jeong H, Melia TJ, et al. The selective macroautophagic degradation of aggregated proteins requires the PI3P-binding protein Alfy. Mol. Cell. 2010; 38:265–279. [PubMed: 20417604]

17. Lin NY, Beyer C, Giessl A, Kireva T, Scholtysek C, Uderhardt S, et al. Autophagy regulates TNFalpha-mediated joint destruction in experimental arthritis. Ann. Rheum. Dis. 2013; 72(5):761–768. [PubMed: 22975756]

18. DeSelm CJ, Miller BC, Zou W, Beatty WL, van Meel E, Takahata Y, et al. Autophagy proteins regulate the secretory component of osteoclastic bone resorption. Dev. Cell. 2011; 21:966–974. [PubMed: 22055344]

19. Kato M, Ospelt C, Gay RE, Gay S, Klein K. Dual role of autophagy in stress-induced cell death in rheumatoid arthritis synovial fibroblasts. Arthritis Rheumat. 2014; 66(1):40–48.

20. Hocking LJ, Mellis DJ, McCabe PS, Helfrich MH, Rogers MJ. Functional interaction between sequestosome-1/p62 and autophagy-linked FYVE-containing protein WDFY3 in human osteoclasts. Biochem. Biophys. Res. Commun. 2010; 402:543–548. [PubMed: 20971078]

21. Thierry-Mieg D, Thierry-Mieg J. AceView: a comprehensive cDNA-supported gene and transcripts annotation. Genome Biol. 2006; 7(Suppl. 1):S12, 1–4. [PubMed: 16925834]

22. Isakson P, Holland P, Simonsen A. The role of ALFY in selective autophagy. Cell Death Differ. 2013; 20:12–20. [PubMed: 22653340]

23. Clausen TH, Lamark T, Isakson P, Finley K, Larsen KB, Brech A, et al. p62/SQSTM1 and ALFY interact to facilitate the formation of p62 bodies/ALIS and their degradation by autophagy. Autophagy. 2010; 6:330–344. [PubMed: 20168092]

24. Takeshita S, Kaji K, Kudo A. Identification and characterization of the new osteoclast progenitor with macrophage phenotypes being able to differentiate into mature osteoclasts. J. Bone Miner. Res. Off. J. Am. Soc. Bone Miner. Res. 2000; 15:1477–1488.

25. Orosco LA, Ross AP, Cates SL, Scott SE, Wu D, Sohn J, et al. Loss of Wdfy3 in mice alters cerebral cortical neurogenesis reflecting aspects of the autism pathology. Nat. Commun. 2014; 5:4692. [PubMed: 25198012]

26. Adamopoulos IE, Chao CC, Geissler R, Laface D, Blumenschein W, Iwakura Y, et al. Interleukin-17A upregulates receptor activator of NF-kappaB on osteoclast precursors. Arthritis Res. Ther. 2010; 12:R29. [PubMed: 20167120]

27. Adamopoulos IE, Sabokbar A, Wordsworth BP, Carr A, Ferguson DJ, Athanasou NA. Synovial fluid macrophages are capable of osteoclast formation and resorption. J. Pathol. 2006; 208:35–43. [PubMed: 16278818]

28. Wu DJ, Dixit N, Suzuki E, Nguyen T, Shin HS, Davis J, et al. A novel in vivo gene transfer technique and in vitro cell based assays for the study of bone loss in musculoskeletal disorders. J. Vis. Exp. 2014; (88):e51810.

29. Bouxsein ML, Boyd SK, Christiansen BA, Guldberg RE, Jepsen KJ, Muller R. Guidelines for assessment of bone microstructure in rodents using micro-computed tomography. J. Bone Miner. Res. Off. J. Am. Soc. Bone Miner. Res. 2010; 25:1468–1486.

30. Ciechanover A. The ubiquitin proteolytic system: from a vague idea, through basic mechanisms, and onto human diseases and drug targeting. Neurology. 2006; 66:S7–S19. [PubMed: 16432150]

31. Klionsky DJ, Emr SD. Autophagy as a regulated pathway of cellular degradation. Science. 2000; 290:1717–1721. [PubMed: 11099404]

32. Johansen T, Lamark T. Selective autophagy mediated by autophagic adapter proteins. Autophagy. 2011; 7:279–296. [PubMed: 21189453]

33. Finley KD, Edeen PT, Cumming RC, Mardahl-Dumesnil MD, Taylor BJ, Rodriguez MH, et al. Blue cheese mutations define a novel, conserved gene involved in progressive neural degeneration. J. Neurosci. Off. J. Soc. Neurosci. 2003; 23:1254–1264.

34. Isakson P, Lystad AH, Breen K, Koster G, Stenmark H, Simonsen A. TRAF6 mediates ubiquitination of KIF23/MKLP1 and is required for midbody ring degradation by selective autophagy. Autophagy. 2013; 9:1955–1964. [PubMed: 24128730]

35. Hacker H, Redecke V, Blagoev B, Kratchmarova I, Hsu LC, Wang GG, et al. Specificity in Toll-like receptor signalling through distinct effector functions of TRAF3 and TRAF6. Nature. 2006; 439:204–207. [PubMed: 16306937]

36. Jin W, Chang M, Paul EM, Babu G, Lee AJ, Reiley W, et al. Deubiquitinating enzyme CYLD negatively regulates RANK signaling and osteoclastogenesis in mice. J. Clin. Investig. 2008; 118:1858–1866. [PubMed: 18382763]

37. Yeremenko N, Noordenbos T, Cantaert T, van Tok M, van de Sande M, Canete JD, et al. Disease-specific and inflammation-independent stromal alterations in spondylarthritis synovitis. Arthritis Rheum. 2013; 65:174–185. [PubMed: 22972410]

38. Martignetti JA, Aqeel AA, Sewairi WA, Boumah CE, Kambouris M, Mayouf SA, et al. Mutation of the matrix metalloproteinase 2 gene (MMP2) causes a multicentric osteolysis and arthritis syndrome. Nat. Genet. 2001; 28:261–265. [PubMed: 11431697]

39. Itoh T, Matsuda H, Tanioka M, Kuwabara K, Itohara S, Suzuki R. The role of matrix metalloproteinase-2 and matrix metalloproteinase-9 in antibody-induced arthritis. J. Immunol. 2002; 169:2643–2647. [PubMed: 12193736]

40. Liu C, Wei Y, Wang J, Pi L, Huang J, Wang P. Carbonic anhydrases III and IV autoantibodies in rheumatoid arthritis, systemic lupus erythematosus, diabetes, hypertensive renal disease, and heart failure. Clin. Dev. Immunol. 2012; 2012:354594. [PubMed: 23049597]

41. Delany AM, Amling M, Priemel M, Howe C, Baron R, Canalis E. Osteopenia and decreased bone formation in osteonectin-deficient mice. J. Clin. Investig. 2000; 105:915–923. [PubMed: 10749571]
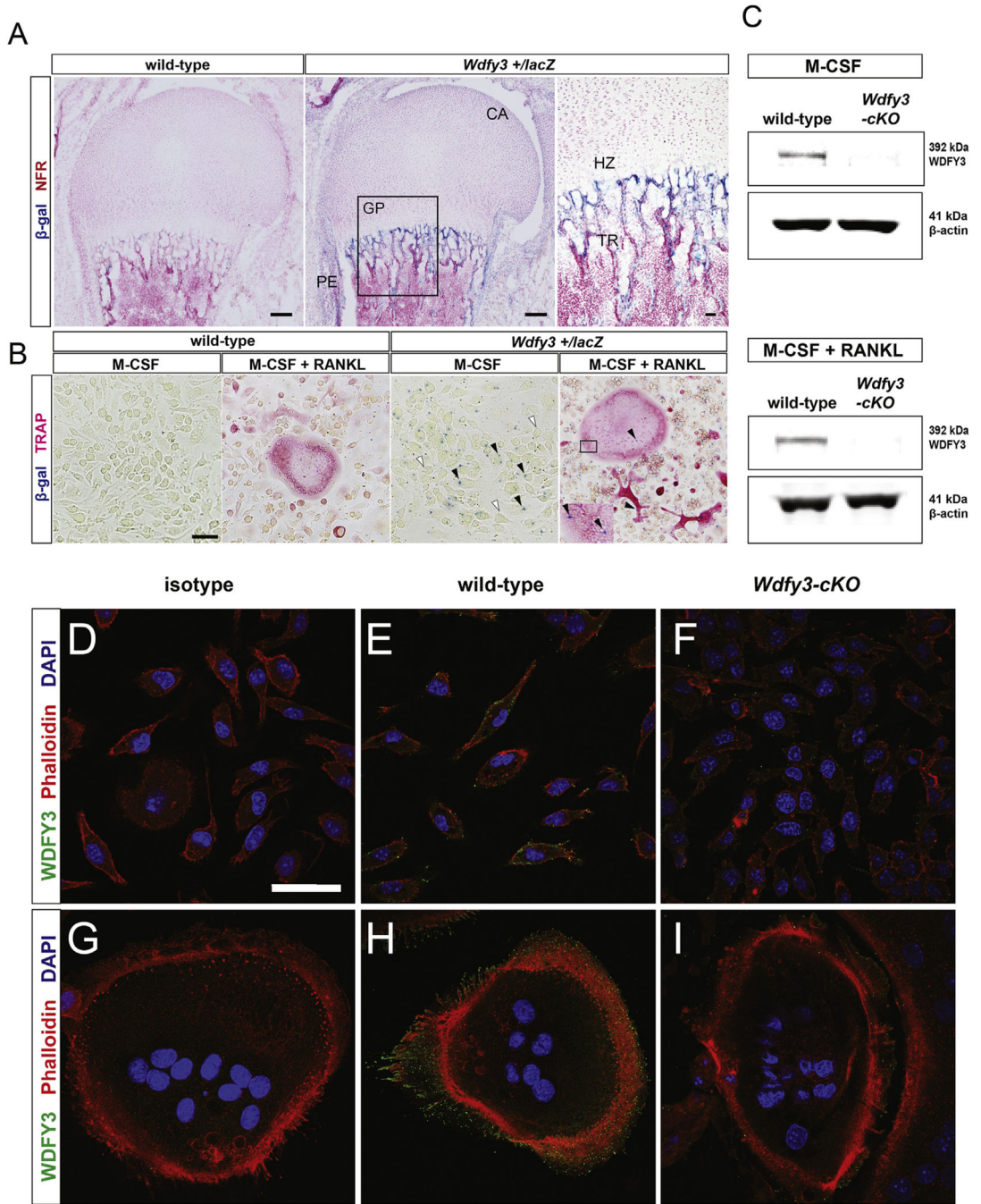
**Fig. 1.**

WDFY3 expression in bone tissues and osteoclasts. (A) X-gal staining counterstained with nuclear fast red (NFR) reveals the distribution of β-gal⁺ cells in the humerus of a newborn (P3) *Wdfy3⁺/lacZ* pup (middle) compared to the wild-type control (left), demonstrating β-gal expression in the cartilage (CA), growth plate (GP), and trabecular (TR) bone. (Boxed area shows β-gal expression at the growth plate of the trabecular bone). (B) Bone marrow-derived macrophages treated with M-CSF in the absence or presence of RANKL were stained with β-gal and counterstained with TRAP. (Black arrowheads indicate β-gal⁺ cells and white

arrowheads indicate β-gal⁻ cells). (C) Western blot analysis of WDFY3 in total cell lysates of bone marrow-derived macrophages treated with M-CSF in the absence or presence of RANKL from wild type or *Wdfy3-cKO* mice. (D–I) Immunofluorescence staining of WDFY3 (green), DAPI (blue), F-actin (red) in bone marrow-derived macrophages (D–F) and multinucleated giant cells (F–I). (For interpretation of the references to colour in this figure legend, the reader is referred to the web version of this article.)
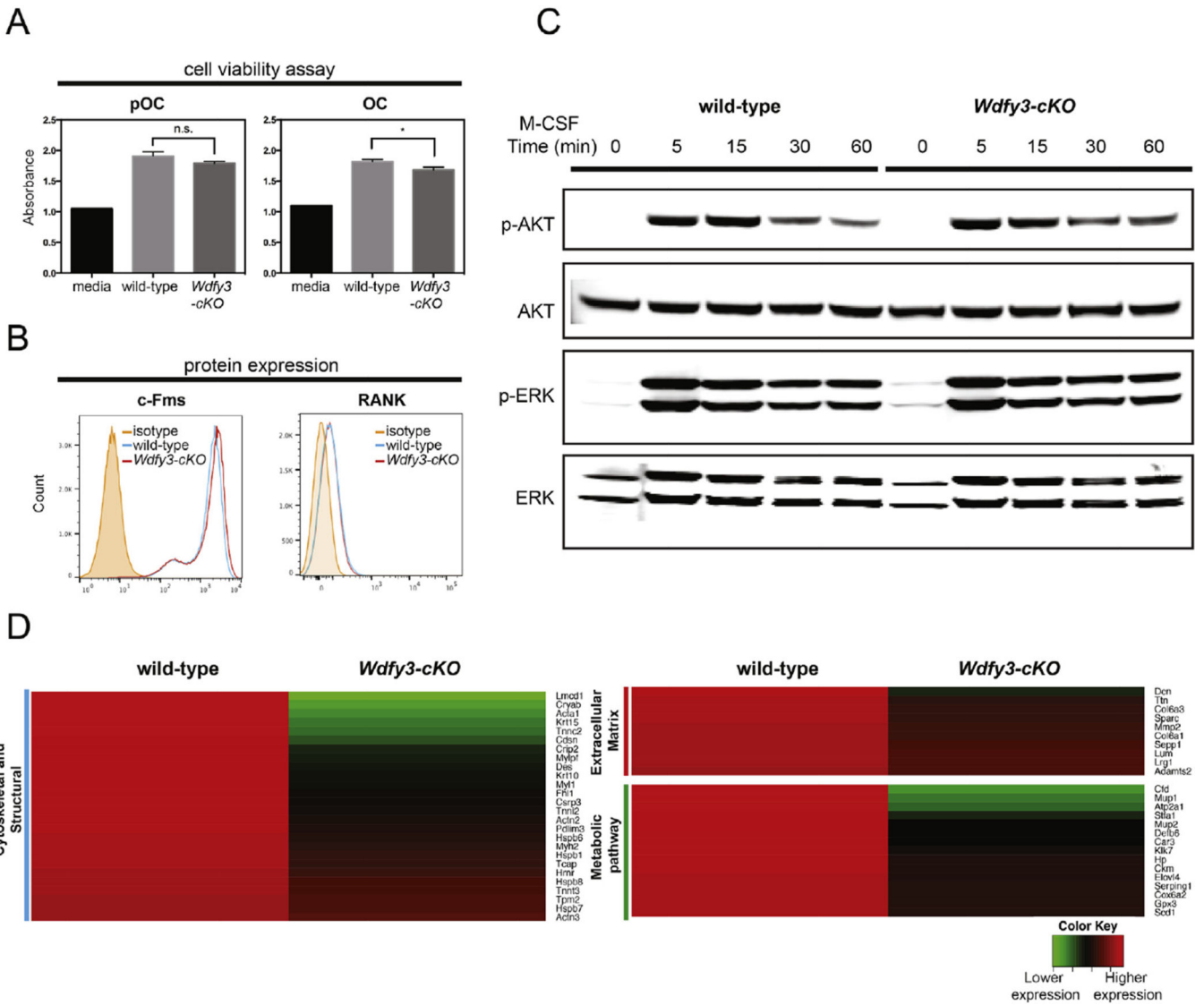
**Fig. 2.**
Phenotyping of WDFY3-deficient bone marrow-derived macrophages. (A) Alamar blue assay of WDFY3-deficient and wild type pre-osteoclasts and osteoclasts cultured for 4 and 8 days with M-CSF in the presence or absence of RANKL respectively. (B) Flow cytometry demonstrated expression of c-Fms and RANK. (C) Western blot analysis of phospho- and total-AKT (pSer473), and ERK (pThr202/Tyr204) in total cell lysates from wild type and *Wdfy3-cKO* BMM culture stimulated with mouse M-CSF (100 ng/ml) for indicated times. (D) Gene expression comparison between WDFY3-deficient TRAP$^+$ multinucleated giant cells and wild type control from microarray analysis. Student *t*-test is used for statistical analysis in A. *$p$ 0.05.
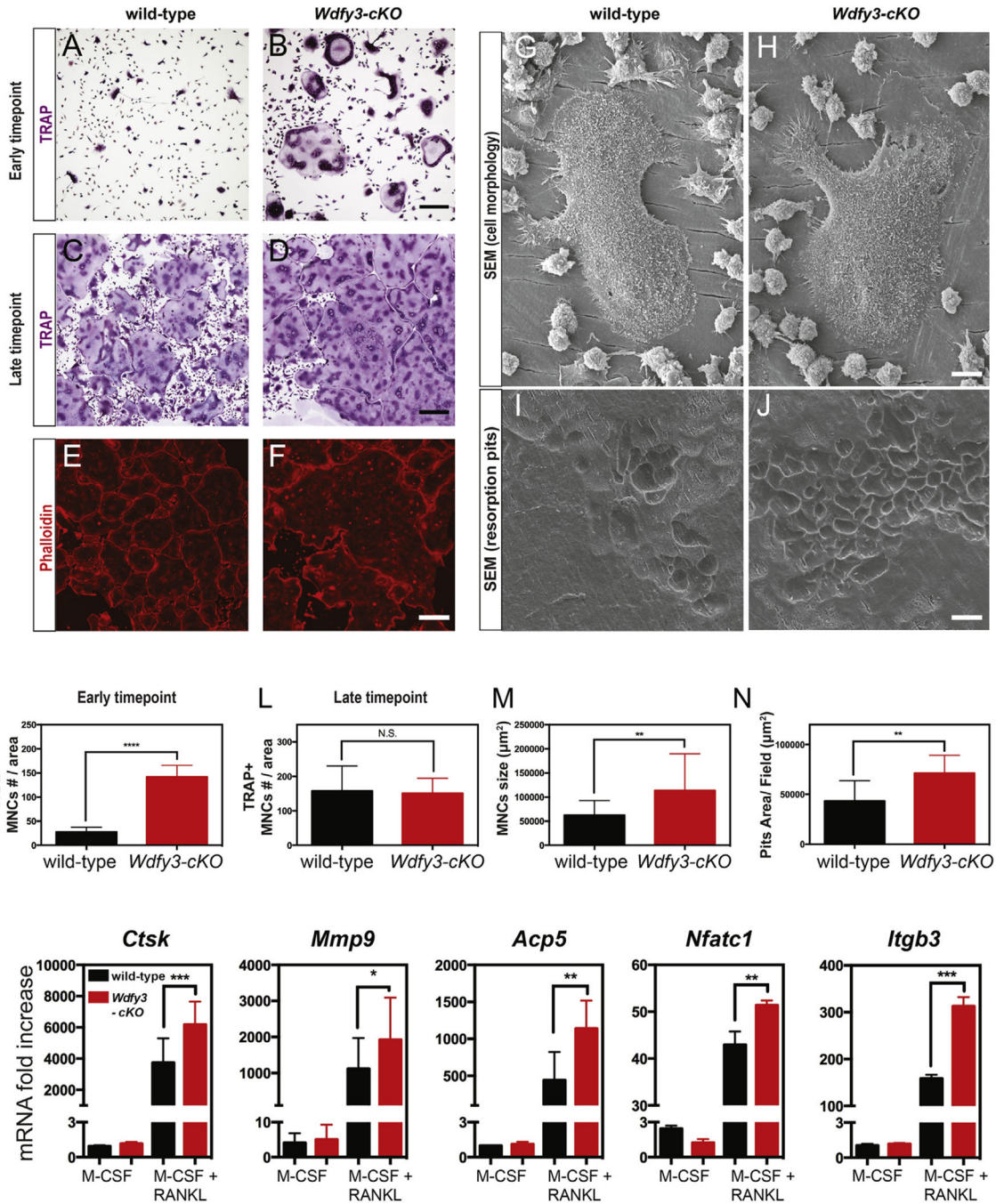
**Fig. 3.**

Enhanced osteoclastogenesis in WDFY3-deficient myeloid cells. Bone marrow cells obtained from femur and tibia bones of wild type mice or *Wdfy3-cKO* mice were differentiated into osteoclasts with the presence of M-CSF and RANKL. (A to F) multinucleated giant cells from *Wdfy3-cKO* mice and wild type mice were analyzed by TRAP staining (A, B, C, D) and phalloidin staining (E, F). (G to J) Scanning electron micrographs of osteoclast cultures from wild type mice (G) or *Wdfy3-cKO* mice (H) demonstrate cell morphology and lacunar resorption activity between wild type (I) and

WDFY3-deficient (J) osteoclasts. (K to M) Quantification of TRAP^{+} multinucleated cells per area (K, L) and multinucleated cells size (M). (N) Quantification of dentine resorption area per field. (O) qPCR analysis of *Ctsk, Mmp9, Acp5, Nfatc1, Itgb3* mRNA levels in the pre-osteoclasts and osteoclasts. Scale bars represent 100 μm in A, B, C, D, E, F, and 10 μm in G, H, I, J. Student *t*-test is used for statistical analysis in K, L, M, N and O. *$p$ 0.05, **$p$ 0.01, ***$p$ 0.001, ****$p$ 0.0001.
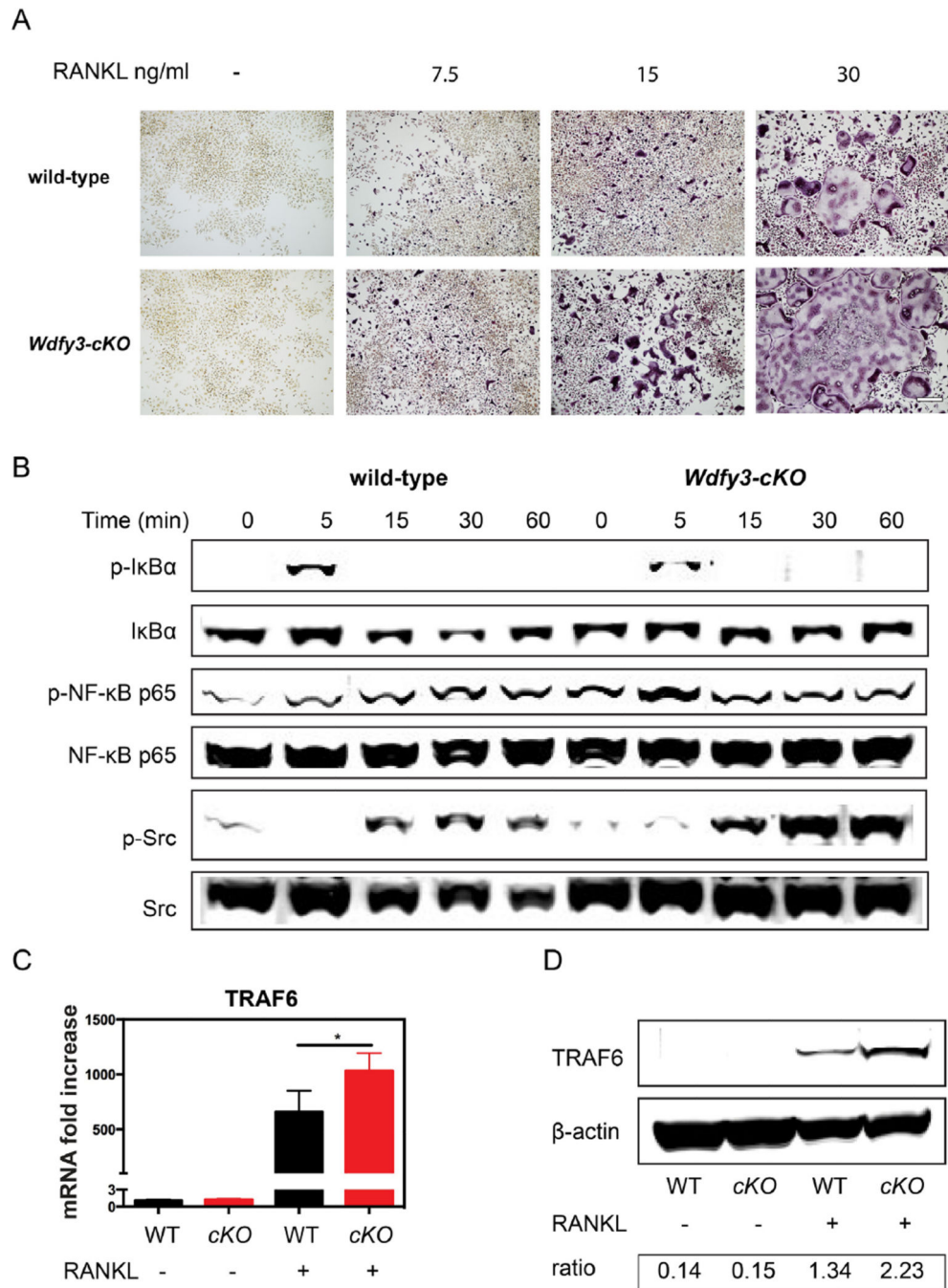
**Fig. 4.**
WDFY3 modulates RANKL-mediated signaling. (A) TRAP staining of wild type and
*Wdfy3-cKO*-derived multinucleated giant cells cultured with M-CSF and increasing
amounts of RANKL for 5 days. (B) Western blot analysis of phospho- and total-IκBα
(pSer32), NF-κB p65 (pSer536), and Src (pY424) in total cell lysates from wild type and
*Wdfy3-cKO* multinucleated giant cell culture stimulated with mouse RANKL (100 ng/ml)
for indicated times. (C) qPCR analysis of TRAF6 message in wild type and *Wdfy3-cKO*
BMMs cell culture treated in the absence or presence of RANKL. (D) Western blot analysis

of TRAF6 in wild type or *Wdfy3-cKO* total cell lysates from BMMs cell culture treated in the absence or presence of RANKL. Scale bar represents 100 μm in A. Student *t*-test is used for statistical analysis in C. *$p$ 0.05.
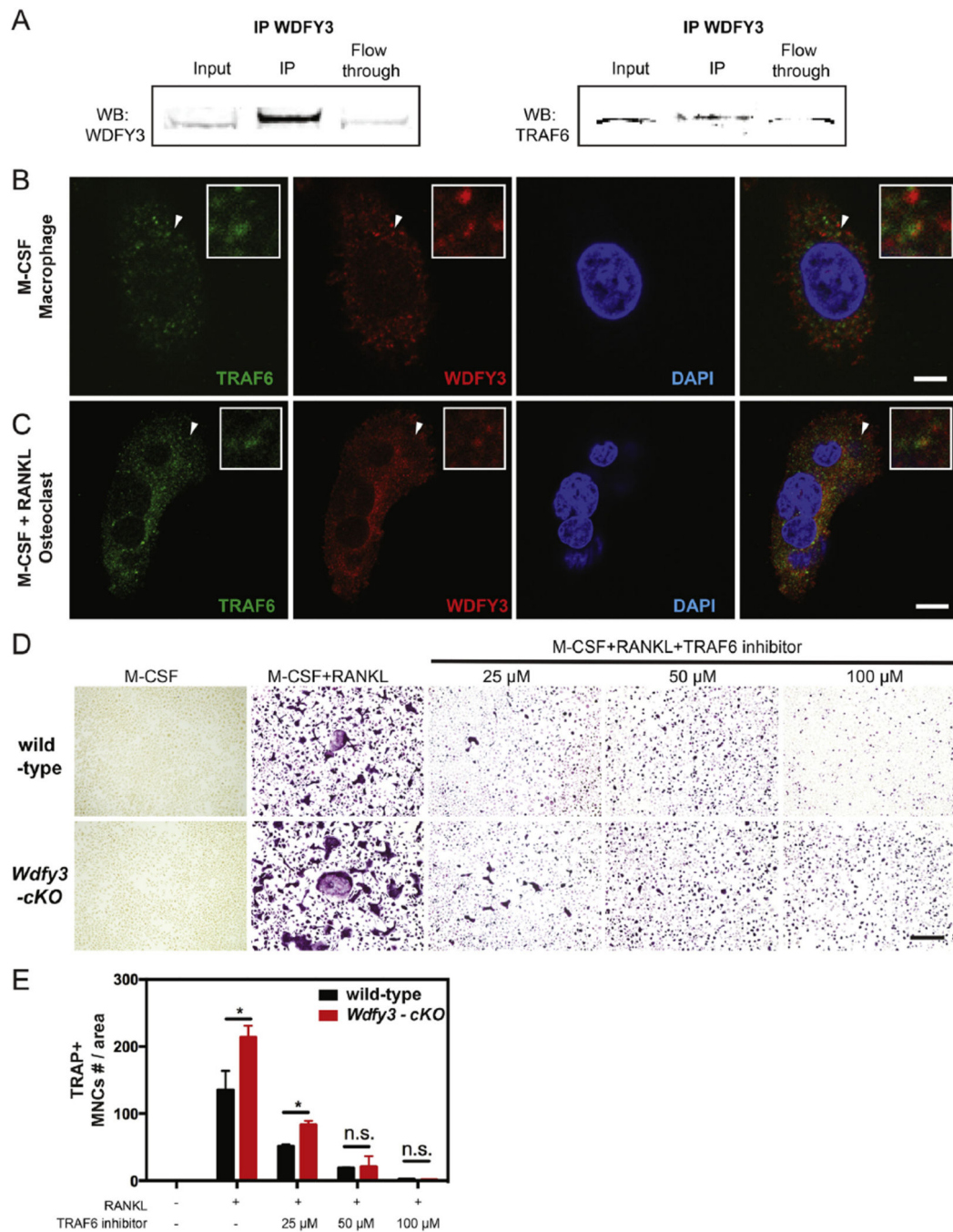
**Fig. 5.**
Enhanced osteoclast differentiation in WDFY3 deficient cell culture is TRAF6 dependent. (A) Total cell lysates from osteoclast cultures co-immunoprecipitated with anti-WDFY3 antibodies and probed with anti-WDFY3 and anti-TRAF6 antibodies. (B) Immunofluorescent photomicrographs of macrophages or (C) multinucleated giant cells were stained with anti-TRAF6 (green), anti-WDFY3 (red), and DAPI (blue). White arrowheads indicated the area where WDFY3 and TRAF6 co-localized. (D) TRAP staining of wild type and *Wdfy3-cKO*-derived multinucleated giant cells cultured with M-CSF and

RANKL and increasing amounts of TRAF6 inhibitor for 5 days, TRAP$^+$ multinucleated giant cells were quantified in (E). Scale bars represent 5 μm in B, 10 μm in C and 300 μm in D. Student $t$-test is used for statistical analysis in E. $*p$ 0.05. (For interpretation of the references to colour in this figure legend, the reader is referred to the web version of this article.)
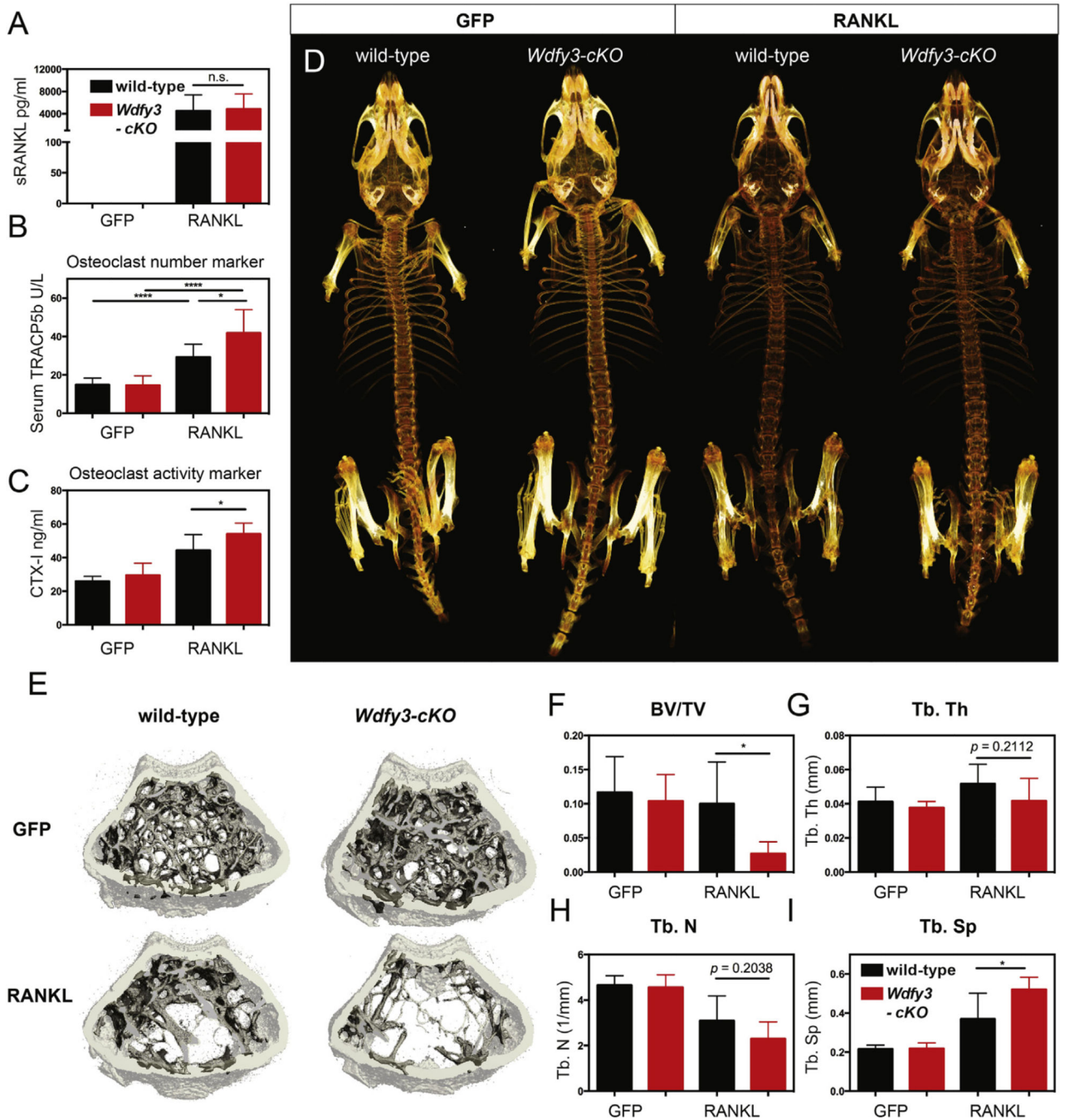
**Fig. 6.**

*Wdfy3-cKO* animals demonstrate exacerbated bone loss in RANKL gene transfer model *in vivo*. (A) RANKL ELISA, (B) Serum TRAP EIA assay, (C) CTX-I EIA assay of serum from RANKL or GFP gene transfer *Wdfy3-cKO* or wild type littermates at day 7-post gene transfer (n = 6–9 animals per group). (D) Whole body or (E) distal femurs MicroCT images of GFP or RANKL gene transfer animals at day 30-post gene transfer. (F to I) MicroCT analysis of distal femurs of GFP gene transfer wild type (n = 8), GFP gene transfer KO (n = 4), RANKL gene transfer wild type (n = 6), RANKL gene transfer KO (n = 5). The results

were pooled from three independent experiments. Student *t*-test is used for statistical analysis in A, B, C, F, G, H, I. *$p$  0.05, **$p$  0.01, ***$p$  0.001, ****$p$  0.0001.